

PAPER • OPEN ACCESS

## Effect of key structures and parameters on dynamic characteristics of three-stage jet-pipe servo valve

To cite this article: Lin Wu *et al* 2019 *IOP Conf. Ser.: Mater. Sci. Eng.* **493** 012161

View the [article online](#) for updates and enhancements.

# Effect of key structures and parameters on dynamic characteristics of three-stage jet-pipe servo valve

Lin Wu<sup>1,2,\*</sup>, Lei Zhang<sup>1,2</sup>, Kuisheng Chen<sup>1,2</sup> and Congchang Zhan<sup>1,2</sup>

<sup>1</sup> Key Laboratory of Metallurgical Equipment and Control Technology, Wuhan University of Science and Technology, Wuhan, Hubei430081, China

<sup>2</sup> Key Laboratory of Mechanical Transmission and Manufacturing Engineering, Wuhan University of Science and Technology, Wuhan, Hubei430081, China

\*Corresponding author e-mail:wulin618wuhan@163.com

**Abstract:** The traditional two-stage electro-hydraulic servo valve cannot meet the needs of production equipment with large flow rate and wide frequency bandwidth. The structure and working principle of the three-stage jet-pipe electro-hydraulic servo valve are described. As the structure of the three-stage valve is complex and many factors influence dynamic characteristics, the main objective of this study is to establish a mathematical model and investigate those factors. In order to advance the local phase, a proportional-derivative correction link is added to the closed-loop transfer function of the three-stage valve. By simulations, the step response curve and open-loop Bode curve are obtained for analysis in the frequency domain and the time domain. The influences of main factors such as flow gain, pressure gain, main spool area, and feedback-rod rigidity on the dynamic response of the valve are analyzed in the time domain. A three-dimensional model of the armature-feedback-rod component is established and is simulated using the Workbench finite-element analysis software. The influences of various structural parameters are analyzed, especially those of the rod area, section shape, length, and material on the feedback rod rigidity.

## 1. Introduction

Electro-hydraulic servo valves (EHSV) have long been regarded as important components in electro-hydraulic servo control systems. Because of their advantages of high precision, reliable operation, light weight, and quick response, they are used widely in ships, aviation, aerospace, and industrial applications [1]. The two types of EHSV that are currently in wide spread use globally are the nozzle-flapper type and the jet-pipe type. Because the traditional two-stage EHSV has low flow rate and small frequency bandwidth, it cannot meet the requirements of high-performance equipment such as analog turntables and material fatigue testing machines. Therefore, because of its higher flow rate and wider frequency bandwidth, the three-stage EHSV is more widely applicable. Over the years, research on the nozzle-flapper EHSV has taken precedence. Therefore, the nozzle flapper is widely used as the pilot stage of the three-stage EHSV. Compared to the nozzle-flapper EHSV, the jet-pipe EHSV has stronger anti-fouling ability, higher flow rate, higher pressure efficiency and volume efficiency of its hydraulic amplifier, and no “full rudder” phenomenon [2]. However, the three-stage jet-pipe EHSV is not widely produced and its comprehensive research has been seldom conducted.

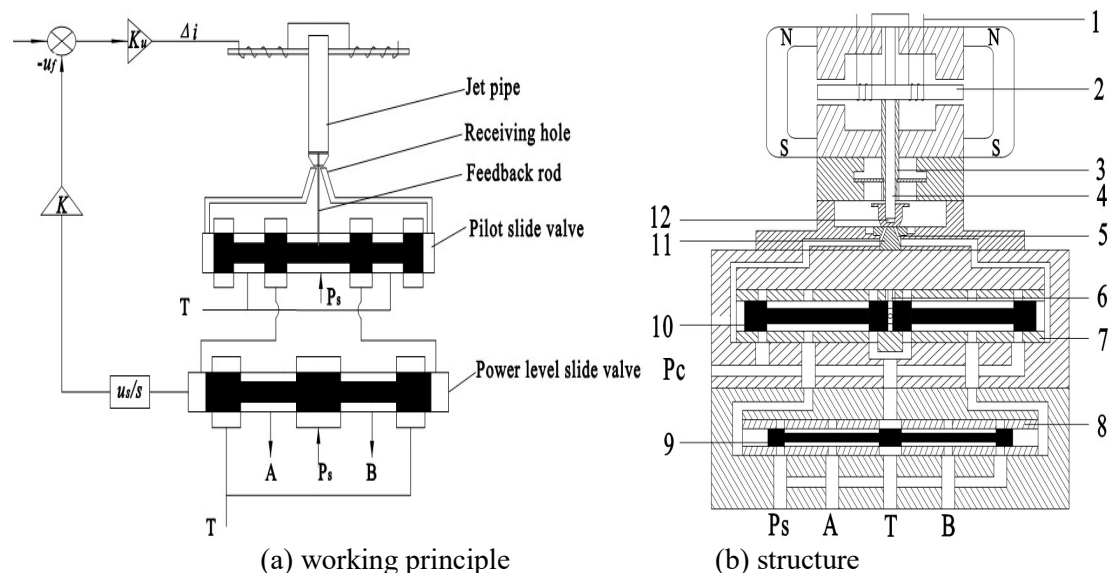


Various scholars have conducted research on the three-stage EHSV. Zhu et al. [3] used the simulation software AMESim to build corresponding simulation models, and they evaluated the structure and various properties of the valve. Wang [4] simulated the three-stage electro-hydraulic sliding valve and analyzed its faults. Huang et al. [5] developed a type of three-stage EHSV and analyzed how the hydraulic power and processing technology influence the valve's performance. Tang et al. [6] used control theory to analyze the dynamic characteristics of the three-stage EHSV, and they designed a proportional–integral–derivative regulator to improve its frequency width. Xu [7] made use of a correction link by improving the three-stage EHSV controller to change the damping and improve the dynamic response. Wang et al. [8] offered an in-depth discussion about the stability of the three-stage EHSV. Through modeling, Xu [9] analyzed the zero-position high-frequency self-excited oscillation of the three-stage EHSV caused by wear of the small ball of the feedback rod. Song [10] derived the mathematical model of the three-stage EHSV, and then obtained its step response curve and open-loop Bode diagram. Liu et al. [11] analyzed how various factors influence the bandwidth and stability of the three-stage EHSV. However, the aforementioned studies were of only the three-stage nozzle-flapper EHSV. S. H. Somashekhar et al. [12] and Li et al. [13] established a model of the two-stage jet-pipe EHSV with force feedback and conducted simulation studies. However, there have been no studies of the three-stage jet-pipe EHSV yet.

The idea of this work is to understand the three-stage jet-pipe EHSV by establishing the mathematical model. A proportional–derivative correction link is added to the closed-loop transfer function, and a three-dimensional model of the armature–feedback-rod component is established. Based on the previous research on EHSV, it is known that the main factors including flow gain, pressure gain, main spool area, and feedback-rod greatly influence the characteristics of EHSV. By taking these factors into account, the dynamic characteristics of the three-stage jet-pipe EHSV is studied.

## 2. Structure and working principle of three-stage jet-pipe electro-hydraulic servo valve

The three-stage jet-pipe EHSV comprises a general two-stage jet-pipe EHSV, a slide valve, and electrical feedback devices for locating. Its working principle and structure are shown in Fig.1.



- 1) coil 2) armature 3) spring pipe 4) jet pipe 5) receiving hole 6) feedback rod 7,8) valve bush 9) power-stage slide valve 10) pilot slide valve 11) receiver 12) nozzle

**Figure 1.** Working principle and structure of three-stage jet-pipe electro-hydraulic servo valve (EHSV).

After the input signal is converted to a current signal and then amplified, it is supplied to the torque motor coil, and an electromagnetic torque is produced to rotate the armature. The armature pushes the jet pipe away from the neutral position, thus the pressure in one receiver hole (that with a larger area of overlap with the jet pipe) is higher than that in the other one, thereby causing the pilot slide valve to move. At this point, the inlet and outlet of the pilot valve are opened and connected with ports A and B, respectively (as shown in Figure 1). Output flow and pressure are generated and act on both ends of the power-stage slide-valve core to force the power-stage slide valve to move. The inlet and outlet of the power-stage slide valve are then opened and connect with ports A and B, respectively. The displacement sensor on the side of the power-stage slide valve converts the detected signal into a feedback voltage signal that is proportional to the displacement of the main valve and adds it to the comparator after amplification. The input signal corrected by the feedback voltage signal is then supplied to the torque motor. When the current is approximately zero, the jet pipe stays at the neutral position and the valve cores do not move. When the load pressure and oil supply pressure are constant, the input voltage is proportional to the output flow rate of the power-stage slide valve.

### 3. Mathematical modeling

#### 3.1. Basic voltage equations

When the armature deflects, the magnetic flux through the air gap changes and a counter electromotive force is generated in the coil. Therefore, part of the amplified input voltage  $u$  is consumed in the resistance of the coil and the internal resistance of the amplifier, and the other part is used to overcome the counter electromotive force. The voltage balance equation of the torque motor circuit is expressed as

$$2K_u u = (R_c + r_p)\Delta i + 2K_b \frac{d\theta}{dt} + 2L_c \frac{d\Delta i}{dt} \quad (1)$$

Where  $K_u$  is the gain of each side of the amplifier,  $u$  is the input voltage signal for each coil,  $R_c$  is the resistance of each coil,  $r_p$  is the amplifier resistance in each coil loop,  $\Delta i$  is the input control current for the torque motor,  $K_b$  is the counter electromotive force constant of each coil,  $\theta$  is the armature rotation angle, and  $L_c$  is the self-induction coefficient of each coil. The Laplace transformation of Eq. (1) is

$$2K_u U = (R_c + r_p)\Delta i + 2K_b s\theta + 2L_c s\Delta i \quad (2)$$

#### 3.2. Equation of motion of torque motor

The torque motor comprises a permanent magnet, a magnetic conducting body, an armature, a control coil, and a spring pipe. The control magnetic flux is generated when the current signal flows through the coil of the torque motor, and is synthesized with the polarizing magnetic flux generated by the permanent magnet in the air gap. Therefore, the magnetic fluxes in the four air gaps between the armature iron and the magnetic conduction body are different. This means that an electromagnetic torque is generated on the armature iron to deflect the armature around the rotating center of the spring pipe. The electromagnetic torque generated on the armature is

$$T_d = K_t \Delta i + K_m \theta \quad (3)$$

Where  $T_d$  is the electromagnetic torque,  $K_t$  is the electromagnetic torque coefficient of the torque motor at the neutral position, and  $K_m$  is the spring stiffness of the torque motor at the neutral position. The equation of motion of the armature subassembly around the rotating center of the spring pipe is

$$T_d = J_a \frac{d^2\theta}{dt^2} + B_a \frac{d\theta}{dt} + K_a\theta + rK_f(r\theta + x_v) \quad (4)$$

Where  $J_a$  is the rotational inertia of the armature subassembly,  $B_a$  is the viscous damping force of the armature subassembly,  $K_a$  is the spring stiffness,  $r$  is the distance between the end of the feedback rod and the center of the spring pipe rotation,  $K_f$  is the feedback-rod rigidity, and  $x_v$  is the displacement of the pilot slide valve. After combining Eqs. (3) and (4) and taking the Laplace transformation, the following equation is obtained:

$$K_t\Delta I = (J_a s^2 + B_a s + K_{mf})\theta(s) + K_f r x_v \quad (5)$$

Where  $K_{mf} = K_a - K_m + r^2 K_f$  is the total stiffness of the torque motor.

### 3.3. Modeling the jet-pipe amplifier

The jet-pipe amplifier comprises the nozzle and the receiver. When the liquid flows out through the nozzle, pressure energy is converted into kinetic energy. After the fluid flow is accepted by the receiver hole, kinetic energy is converted into pressure energy to drive the pilot slide valve. It is difficult to analyze theoretically the energy conversion of the jet-pipe amplifier. According to the relationship between the output flow/pressure of the jet-pipe amplifier and the deflection displacement of the jet pipe, the following mathematical model is established when ignoring other nonlinear factors and considering the deflection displacement to be small:

$$\begin{cases} x_f = r_0 \theta \\ Q_L = K_{qs} x_f - K_{cs} P_L \end{cases} \quad (6)$$

Here,  $x_f$  is the deflection displacement of the jet pipe,  $r_0$  is the deflection radius of the jet pipe,  $Q_L$  is the output flow of the jet pipe,  $K_{qs}$  is the flow gain of the jet pipe,  $K_{cs}$  is the flow-pressure coefficient of the jet pipe, and  $P_L$  is the output pressure of the jet pipe. The Laplace transformations of Eq. (6) are

$$\begin{cases} X_f = r_0 \theta(s) \\ Q_L = K_{qs} X_f - K_{cs} P_L \end{cases} \quad (7)$$

The structure of the jet-pipe servo valve (SV) differs from that of the nozzle-flapper SV, and their models are established differently. The stability of the pressure feedback loop in the SV has a great influence on the stability of the whole valve. To minimize the influence of the loop, it is necessary to adjust the model parameters by changing the open-loop gain of the loop to make the loop approximately open. However, there is no such pressure feedback loop in the jet-pipe SV, thus there is no need to adjust the model parameters. In addition, the jet-pipe SV differs from the nozzle-flapper SV in that the jet-pipe amplifier converts energy. To make the simulation convenient, this energy conversion is not taken into account; the nonlinear factors caused by energy conversion are ignored, and the model of the jet amplifier is linearized. As such, this model does not reflect the true situation exactly. Therefore, the subsequent simulation study did not consider how energy conversion affects the dynamic response of the valve.

### 3.4. Mathematical model of pilot slide valve

The pilot-stage spool valve is a type of a zero-opening four-sided spool. By ignoring the pressure loss and the leakage of the spool and by assuming that the pressure in each chamber is equal when the spool is static, the flow equation of the slide valve is

$$Q_L = A_v \frac{dx_v}{dt} \quad (8)$$

Where  $A_v$  is the core area of the pilot slide valve. To drive the spool to move, the pressure applied to both ends of the spool valve must overcome the mass of the valve core, the inertial force, the steady-state flow force, the feedback force of the feedback rod, and the viscous damping force[14]. Because the transient flow force and friction force are too small, the following equation is established by ignoring them:

$$A_v P_L = M_v \frac{d^2 x_v}{dt^2} + B_v \frac{dx_v}{dt} + K_f x_v + K_f r \theta + 0.43W(P_s - P_b)x_v \quad (9)$$

Where  $M_v$  is the mass of the pilot slide valve,  $B_v$  is the viscous damping coefficient of the pilot slide valve,  $W$  is the area gradient of the pilot slide valve, and  $P_b$  is the load pressure in the two cavities of the power-stage slide valve. The steady-state flow force in the above equation is related to the variables  $P_b$  and  $x_v$ . Therefore, if the load pressure of the power-stage slide valve is assumed to be pure inertia, Eq. (9) can be linearized about  $x_{v0}$  and  $P_{b0}$ . Because  $P_{b0}$  is zero in the steady state, the Laplace transformations of Eqs. (8) and (9) can be obtained as

$$\begin{cases} Q_L = A_v s X_v \\ A_v P_L = [M_v s^2 + B_v s + 0.43W P_s + K_f] X_v - 0.43W X_{v0} P_b + K_f r \theta \end{cases} \quad (10)$$

### 3.5. Mathematical model of power-stage slide valve

The output flow of the pilot slide valve drives the motion of the power-stage slide valve, and its linearized flow equation is

$$q_L = K_{qp} x_v - K_{cp} P_b \quad (11)$$

For the pilot slide valve, its output flow, flow gain, and flow-pressure coefficient are  $q_L$ ,  $K_{qp}$ , and  $K_{cp}$ , respectively. Assuming that the initial volumes of the two working chambers of the power-stage slide valve are equal and ignoring the leakage flow, the continuity equation of the power-stage slide valve is

$$q_L = A_p \frac{dx_p}{dt} + \frac{V_t}{4\beta_e} \frac{dP_b}{dt} \quad (12)$$

Where  $A_p$  is the core area of the power-stage slide valve,  $x_p$  is the displacement of the power-stage slide valve,  $V_t$  is the total compression area, and  $\beta_e$  is the effective volume elastic modulus. Generally, the loads acting on the power-stage slide valve include inertia, viscous damping, and the steady-state hydraulic force. Thus the force balance equation of the power-stage slide valve is

$$A_p P_b = m_t \frac{d^2 x_p}{dt^2} + B_p \frac{dx_p}{dt} + 0.43 W_p P_s x_p, \quad (13)$$

Where  $m_i$  is the mass of the power-stage slide valve and  $W_p$  is the area gradient of the power-stage slide valve. The Laplace transformations of Eqs. (11)–(13) are

$$\begin{cases} q_L = K_{qp} X_v - K_{cp} P_b \\ q_L = A_p s X_p + \frac{V_t}{4\beta_e} s P_b \\ A_p P_b = m_t s^2 X_p + B_p s X_p + 0.43 W_p P_s X_p \end{cases} \quad (14)$$

#### 4. Dynamic performance simulation

In practical applications, the general way to improve the dynamic response of the system is to increase the open-loop gain of the system. However, that method reduces the amplitude margin and the phase margin of the system and makes the system unstable. To achieve the celerity, accuracy, and stability for the three-stage valve, a proportional-derivative (PD) correction link can be added to the forward channel to advance the local phase of the system, thereby improving the stability of the system. The PD correction link is easily realized via appropriate circuits in the electric controller. Based on Eqs. (2), (5), (7), (10), and (14), the system block diagram established by adding a PD correction link is as shown in Fig.2.

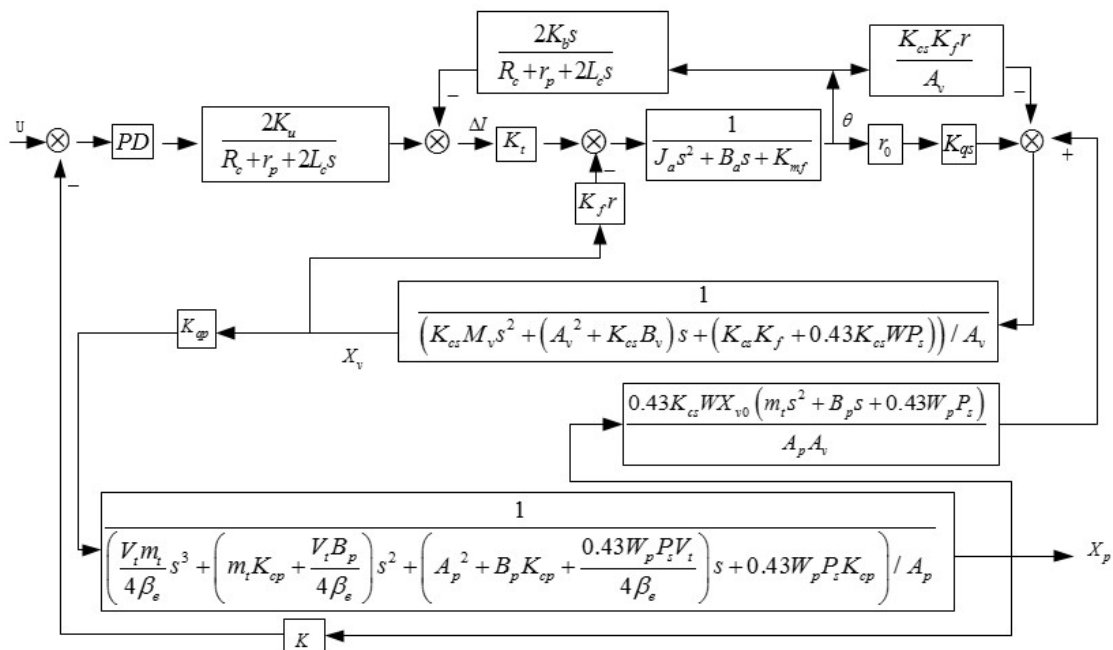


**Figure 2.** System block diagram of three-stage jet-pipe EHSV.

Herein, Simulink is used to simulate the dynamic characteristics of the three-stage jet-pipe EHSV. Simulink is a MATLAB visual simulation tool and a software package for modeling, simulating, and analyzing dynamic systems. It is widely used to model and simulate linear systems, nonlinear systems, digital control, and digital signal processing. Moreover, it provides an integrated environment for the modeling, simulation, and comprehensive analysis of dynamic systems. In that environment, a complex system can be constructed not with a large number of writing procedures but with only simple, intuitive

mouse operations[15]. Simulink has the advantages of being widely adaptable, having a clear structure and process, offering fine simulation results, being close to reality, and being highly efficient and flexible. The simulation parameters are shown in Table 1.

**Table 1.** Physical parameters and values

Parameter	Value
Gain of each side of the amplifier	$K_u=5$
Resistance of each coil	$R_c=100\ \Omega$
Amplifier resistance in each coil loop	$r_p=900\ \Omega$
Counter electromotive force constant of each coil	$K_b=2.18\ \text{N}\cdot\text{m}\cdot\text{A}^{-1}$
Electromagnetic torque coefficient of torque motor at neutral position	$K_t=2.18\ \text{N}\cdot\text{m}\cdot\text{A}^{-1}$
Self-induction coefficient of each coil	$L_c=6.7\times 10^5\ \text{H}$
Spring stiffness of armature subassembly	$K_a=9.91\ \text{N}\cdot\text{m}\cdot\text{rad}^{-1}$
Spring stiffness of torque motor	$K_m=7.94\ \text{N}\cdot\text{m}\cdot\text{rad}^{-1}$
Distance between end of feedback rod and center of spring pipe rotation	$r=0.0222\ \text{m}$
Feedback-rod rigidity	$K_f=2,000\ \text{N}\cdot\text{m}^{-1}$
Rotational inertia of armature subassembly	$J_a=1.05\times 10^{-6}\ \text{kg}\cdot\text{m}^2$
Viscous damping force of armature subassembly	$B_a=0.0021$
Deflection radius of jet pipe	$r_0=0.0089\ \text{m}$
Flow gain of jet pipe	$K_{qs}=4.28\times 10^{-2}\ \text{m}^2\text{s}^{-1}$
Flow-pressure coefficient of jet pipe	$K_{cs}=3.37\times 10^{-13}\ \text{m}^3\text{Pa}^{-1}\text{s}^{-1}$
Core area of pilot slide valve	$A_v=1.76\times 10^{-5}\ \text{m}^2$
Mass of pilot slide valve	$M_v=0.07\ \text{kg}$
Viscous damping coefficient of pilot slide valve	$B_v=1.01$
Displacement of pilot slide valve	$x_{v0}=0.75\times 10^{-3}\ \text{m}$
Flow gain of pilot slide valve	$K_{qp}=0.433\ \text{m}^2\text{s}^{-1}$
Flow-pressure coefficient of pilot slide valve	$K_{cp}=1.53\times 10^{-12}\ \text{m}^3\text{Pa}^{-1}\text{s}^{-1}$
Core area of power-stage slide valve	$A_p=7.14\times 10^{-4}\ \text{m}^2$
Total compression area	$V_f=14.28\times 10^{-5}\ \text{m}^3$
Effective volume elastic modulus	$\beta_e=8\times 10^8\ \text{Pa}$
Mass of power-stage slide valve	$m_f=0.6\ \text{kg}$
Viscous damping coefficient of power-stage slide valve	$B_p=47\ \text{N}\cdot\text{s}\cdot\text{m}^{-1}$
Inlet pressure	$P_s=21\times 10^6\ \text{Pa}$

As can be seen from Fig.2, the transfer function of the system is quite complex. Previous studies often simplified the transfer function to some extent when analyzing the dynamic characteristics. However, because of the complex structure of the three-stage SV, such simplification may influence the SV greatly. Therefore, the simulation model is built according to the block diagram, and  $K_p=0.8$  and  $K_d=0.0015$  in the PD correction link were obtained through trial and error. Through simulation, the step response curve and the open-loop Bode diagram of the system before and after correction can be obtained, as shown in Figs. 3–5.



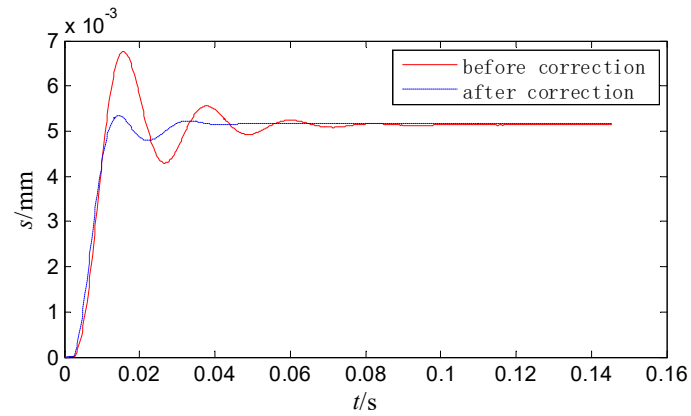


**Figure 3.** Step response curve.

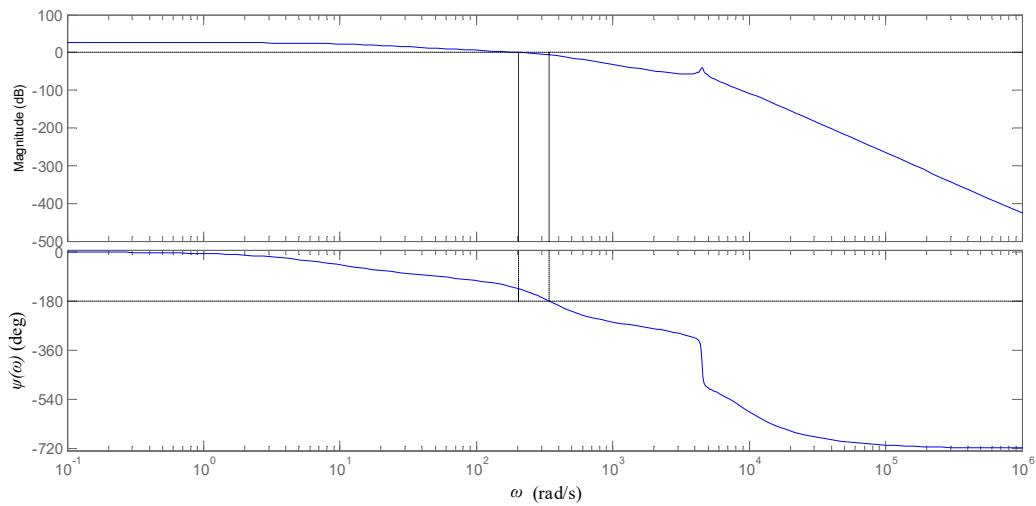


**Figure 4.** Open-loop Bode diagram before correction.

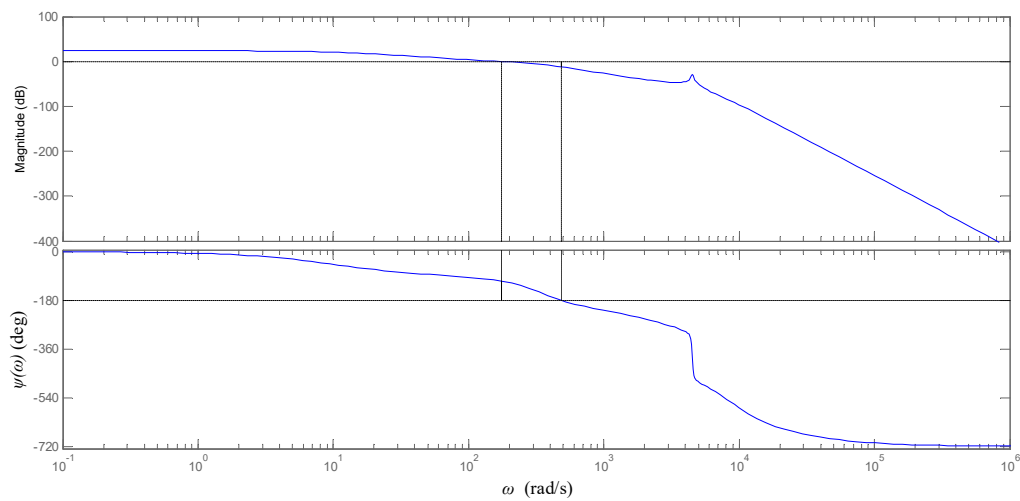


**Figure 5.** Open-loop Bode diagram after correction.

As can be seen from Fig.3, the rise time, peak time, and adjustment time of the system are 9.8, 14.7, and 80 ms, respectively, before the correction and 10.8, 12.1, and 40 ms, respectively, after the

correction. The overshoot is large ( $\sim 35\%$ ) before the correction but is only around  $0.7\%$  after the correction. Figure 4 shows that the amplitude margin increased from  $5.92\text{ dB}$  to  $11.9\text{ dB}$  and the phase margin increased from  $45.7^\circ$  to  $72^\circ$  after adding the correction link. It is concluded that the system stability and response speed are improved.

## 5. Parametric impact analysis

Because of the complex structure of the three-stage EHSV, many factors influence its dynamic performance. The key factors are the flow gain  $K_{qs}$ , the pressure gain  $K_{cs}$ , and the core area  $A_p$  of the power-stage slide valve.  $K_{qs}$  affects the open-loop gain of the system,  $K_{cs}$  affects the positive feedback of the system and the dynamic response of the jet amplifier, and  $A_p$  affects both the open-loop gain and positive feedback of the system. Here, how these factors influence the dynamic performance of the three-stage valve is analyzed.

### 5.1. Influence of flow gain of jet amplifier on valve

The step response curves for  $K_{qs} = 3.17 \times 10^{-2}$ ,  $4.28 \times 10^{-2}$ , and  $5.32 \times 10^{-2} \text{ m}^2 \text{ s}^{-1}$  are shown in Fig.6. With increasing flow gain of the jet amplifier, the open-loop gain of the system clearly increases and the system response becomes faster. Although the response of the system is accelerated, the overshoot is increased and the system stability is reduced. In addition, when the system reaches the steady state, the displacement decreases with increasing flow gain. This is because the feedback function of the system is constant, thus the steady-state deviation and error of the system are smaller when the gain is larger. It is concluded that the response is faster, the steady-state error is smaller, and the system is more unstable when the flow gain is larger.

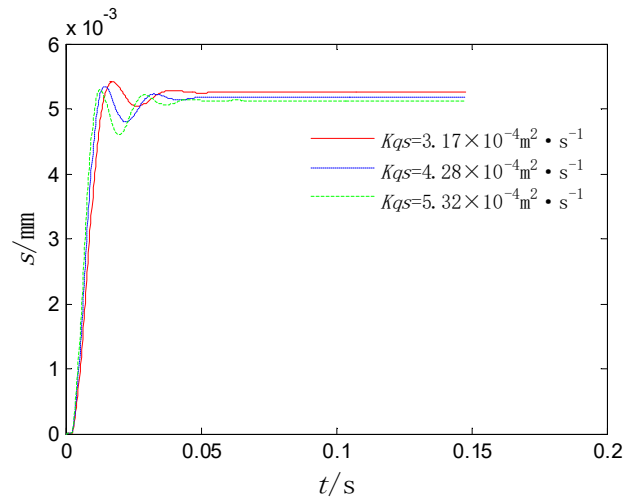


**Figure 6.** Step response curves for different values of  $K_{qs}$ .

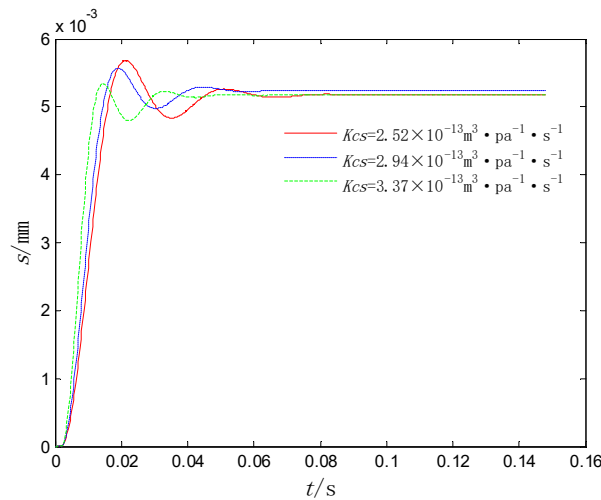


**Figure 7.** Step response curves for different values of  $K_{cs}$ .

### 5.2. Influence of pressure gain of jet amplifier on valve

The step response curves for  $K_{cs} = 2.52 \times 10^{-13}$ ,  $2.94 \times 10^{-13}$ , and  $3.37 \times 10^{-13} \text{ m}^3 \text{ s}^{-1} \text{ Pa}^{-1}$  are shown in Fig.7. With decreasing pressure gain of the jet amplifier, the rise time and adjustment time of the system are clearly longer and the system is more unstable. The reason is that the damping ratio of the jet amplifier and the open-loop gain of the system increase as the pressure gain decreases. Although increasing the damping ratio can reduce the overshoot of the system, the main factor that affects the system instability is the open-loop gain. In the same way, increasing the open-loop gain can accelerate the response of the system, but the main factor affecting the response speed of the system is the damping ratio.

### 5.3. Influence of power-stage core area on valve

The step response curves for  $A_p = 5.6$ ,  $7.14$ , and  $10.2 \text{ cm}^2$  are shown in Fig.8. When the core area of the power-stage valve is smaller, the open-loop gain of the system and the rise time increase, but the stability and steady-state error of the system decrease. Meanwhile, a smaller core area increases the positive feedback of the system, also resulting in system instability. However, making the area too large slows down the response of the valve and increases the size and mass of the valve core.

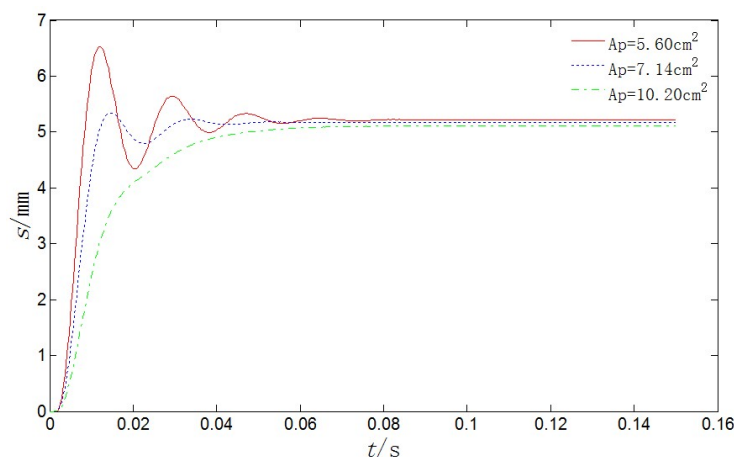


**Figure 8.** Step response curves for different values of  $A_p$ .

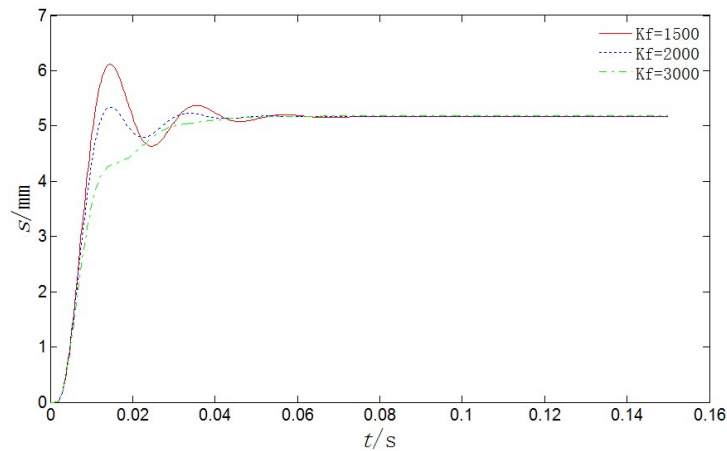


**Figure 9.** Step response curves for different values of  $K_f$ .

#### 5.4. Influence of feedback-rod rigidity on valve

In addition to the above parameters, the stiffness of the feedback rod also has a great impact on the dynamic characteristics of the valve. To study the influence of  $K_f$ , the other parameters are held constant. The step response curves for  $K_f=1,500$ ,  $2,000$ , and  $3,000 \text{ N m}^{-1}$  are shown in Fig.9. With increasing feedback-rod rigidity, the system stability is clearly better, the adjustment time is reduced, the overshoot decreases, but the rising time increases. When the feedback-rod rigidity is too small, the frequency of the feedback rod increases, which is not conducive to the stability of the valve. When the feedback-rod rigidity is too large, it is not conducive to rapid feedback motion. Therefore, it is necessary to determine the feedback-rod rigidity reasonably.

When a current is applied to the coil, the generated electromagnetic torque causes the armature to deflect around the rotating center of the spring pipe and drives the jet pipe to deflect in the same direction as that of the armature. Simultaneously, the inlet pipe, the zeroing wire, the spring pipe, and the feedback rod produce an opposite torque to hinder the deflection. The jet-pipe SV is in equilibrium when the armature–feedback-rod subassembly reaches balance. Because the feedback-rod rigidity has an important influence on the dynamic response of the three-stage jet-pipe EHSV, it is necessary to study the former in depth. Herein, ANSYS Workbench is used to conduct finite-element analysis of feedback rods with different areas, sections, lengths, and materials.

The armature–feedback-rod subassembly includes the zeroing wire, inlet pipe, armature, reed, jet pipe, spring pipe, nozzle, and feedback-rod subassembly. A three-dimensional model of the armature–feedback-rod subassembly is established, and two equal forces in opposite directions are applied to each side of the armature, respectively. A force is applied to the end of the feedback rod to prevent the armature from deflecting. The ends of the inlet pipe, the zeroing wire, the spring pipe, and both sides of the reed are set as full constraints, and the forces on both sides of the armature remain unchanged. By changing the force applied to the end of the feedback rod, the displacements of the jet pipe and the valve core are obtained [16-20]. The deformation of the feedback rod is shown in Figure 10, and the displacements of the jet pipe and valve core under different areas, cross-section shapes, lengths, and materials of the feedback rod are shown in Figs.11–14.

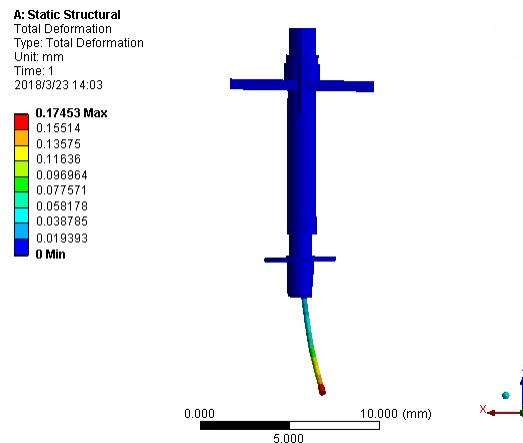


**Figure 10.** Deformation diagram of feedback rod.

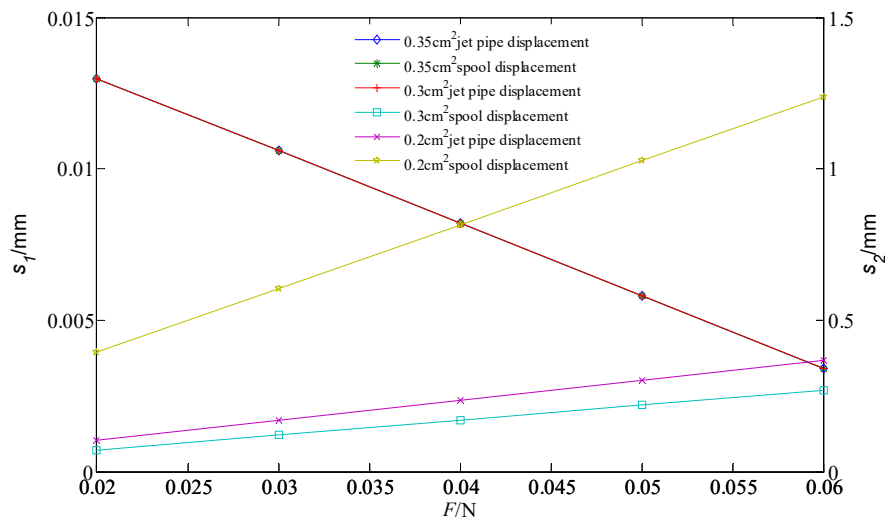
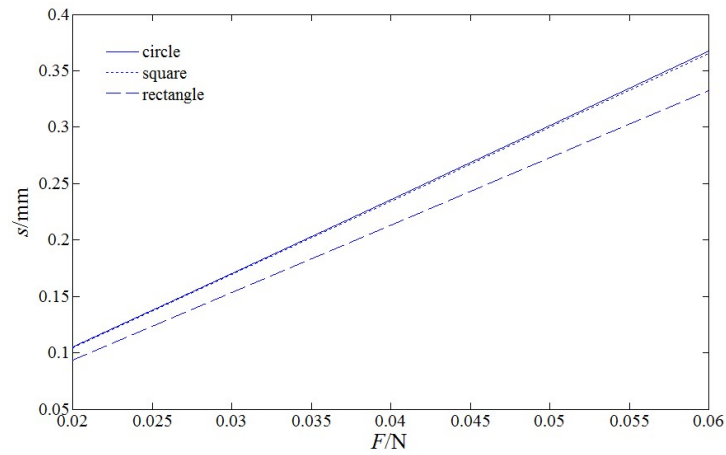


**Figure 11.** Displacements of jet pipe and spool under different areas of feedback rod.

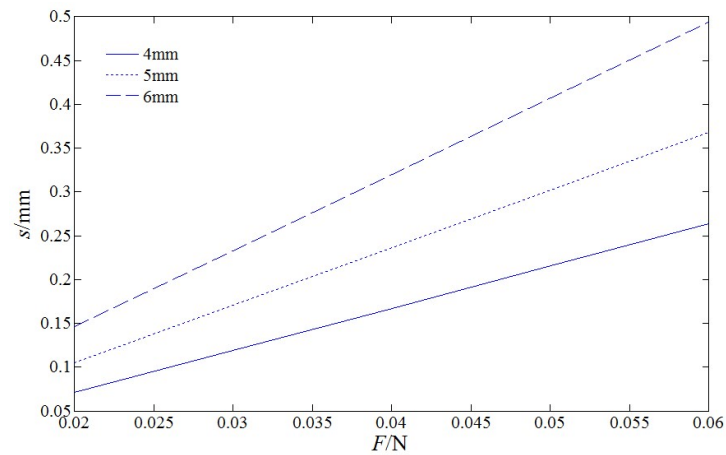
It can be seen from Fig.10 that the feedback rod is deformed under the simultaneous actions of the electromagnetic moment and the feedback force. The deformation of the end of the feedback rod is the maximum and equals the displacement of the spool. The displacement of the jet pipe is assumed to be positive to the left, whereas the displacement of the valve core is positive to the right.

Fig.11 shows that under different feedback forces, the displacement of the jet pipe decreases linearly whereas that of the valve core increases linearly. The armature–feedback-rod subassembly is taken as a whole. Although the area of the feedback rod differs, the force acting on the jet pipe is the same for the same feedback force. Thus the displacement of the jet pipe does not change with the area of the feedback rod. According to Newton's second law, the force acting on the upper part of the feedback rod remains unchanged, making the feedback rod equivalent to a cantilever beam. The displacement of the valve core decreases with increasing area of the feedback rod as the section inertia moment increases. Under the same force, the smaller the displacement, the greater the rigidity.

Similarly, changing the property of the feedback rod does not affect the displacement of the jet pipe but affects only the displacement of the valve core. The displacements of the valve core under different section shapes, lengths, and materials are shown in Figs.12–14, respectively.



**Figure 12.** Displacement of spool with differing section shape of feedback rod.



**Figure 13.** Displacement of spool with differing length of feedback rod.

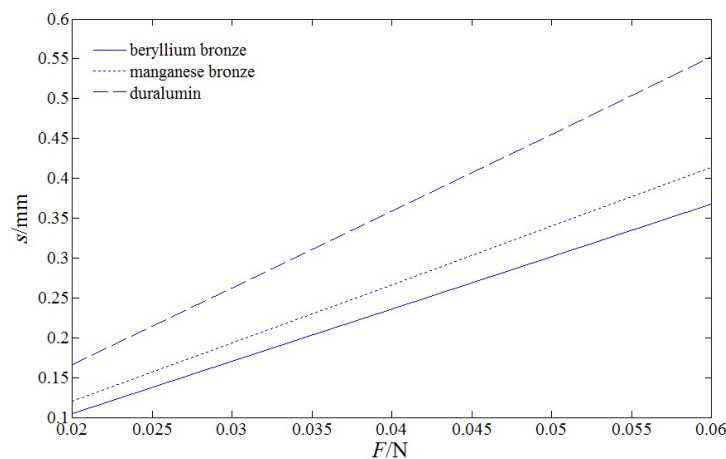


**Figure 14.** Displacement of spool with differing material of feedback rod.

As shown in Fig.12, for a given section area and feedback force, the displacement of the valve core with a rectangular section is the smallest, whereas that of the valve core with a circular section is the largest. The reason for this is that the moment of inertia is the largest and the smallest for the rectangular

section and the circular section, respectively. Therefore, for a given force, the rigidity of the rectangular section increases as the displacement of the valve decreases.

As shown in Fig.13, the displacement of the valve core decreases as the length of the feedback rod decreases. This is because the deflection of a cantilever beam is proportional to its extension length. Therefore, for a given force, the shorter the extension, the shorter the displacement of the valve, that is, the greater the rigidity.

It can be seen from Fig.14 that for a given force, the displacement of the valve core is the smallest when the material of the feedback rod is beryllium bronze. When the material of the feedback rod is hard aluminum alloy, the displacement of the valve core is the largest. The elastic modulus of hard aluminum alloy is the largest whereas that of beryllium bronze is the smallest. For a cantilever beam, the deflection is inversely proportional to the elastic modulus of the material. The greater the elastic modulus of the feedback-rod material, the smaller the valve displacement, thus the greater the rigidity. Therefore, the greater the inertia moment of the feedback-rod section, the smaller the extension, and the larger the elastic modulus, the greater the stiffness of the feedback rod, resulting in a better dynamic response of the three-stage SV.

## 6. Conclusion

The following conclusions can be drawn from modeling and simulating the three-stage jet-pipe EHSV and analyzing the time domain and frequency domain.

1. Adding a PD correction link not only greatly reduces the adjustment time of the EHSV but also makes its amplitude margin exceed 6 dB and its phase margin exceed 60°. The stability of the system is enhanced.

2. The flow of the jet-pipe amplifier is the key factor influencing the open-loop amplification coefficient of the system. Increasing the flow gain increases the loop amplification coefficient, thereby reducing the response time and adjustment time of the system. Consequently, the stability worsens and the steady-state error decreases.

3. The pressure gain of the jet-pipe amplifier affects mainly the damping ratio of the system. Increasing the pressure gain reduces the damping ratio, thereby reducing the rise time and adjustment time of the system and accelerating its response.

4. The area of the power slide-valve core has a major impact on the open-loop amplification coefficient and the positive feedback in the system. With decreasing area of the valve core, the amplification coefficient increases and the response of the system becomes faster. Simultaneously, the positive feedback effect is enhanced, making the system unstable and reducing the steady-state error.

5. The influence of the feedback-rod rigidity on the system is manifold. By increasing the feedback-rod stiffness, the adjustment time and the overshoot are reduced, the stability of the system is increased, but the rise time of the system is reduced. Under the actions of torque and feedback force, the deformation at the end of the feedback rod equals the displacement of the main valve core, and can be simplified as the force deformation of a cantilever beam. Therefore, the feedback-rod rigidity can be improved by increasing the section inertia moment and elastic modulus and decreasing the extension length.

The present modeling and simulation of the three-stage jet-pipe EHSV offers a theoretical basis for designing and improving the three-stage EHSV.

## Acknowledgments

This work was financially supported by Natural Science Foundation of Hubei Province (ZRZ2014000117) and National Natural Science Foundation (51475338).

## References

- [1] Shanghai 704 Institute Hengtuo Development Co., Ltd. Servo-valve Department. Special lecture on jet pipe electro-hydraulic servo valve. Chin.Hydraul.Pneumat. 9 (2009) 88-89.
- [2] Fang. Q. The application and development trend of electro-hydraulic servo valve of jet pipe. Fifth

- Chinese Ship and Marine Engineering Development Forum and the Marine Engineering Deck Cabin Mechanical Technology Development Forum. Nanjing, 2013, pp. 90–102.
- [3] Zhu XB and Chen KS. New stimulation & research of the three stage servo valve. *Machine Tool Hydraul.* 2 (2005) 97-98.
- [4] Wang DW. Flow field characteristics of three-stage servo valve and fault simulation analysis. Harbin: Harbin Institute of Technology. 2013.
- [5] Huang XS, Qu LP, and Shui ZF. The design of three-stage servo valve with electrical position feedback. *Machine Tool Hydraul.* 2 (2010) 53-55.
- [6] Tang JM, Zhu SG. To improve the dynamic response of three-stage electro-hydraulic servo valve. *Chin.Hydraul.Pneumat.* 4 (1983) 8-12.
- [7] Xu ML. A discussion on improving the dynamic response of three-level electro-hydraulic servo valve with correction. *Aviation Precision Manufac.Technol.* 5 ( 1997) 36-39.
- [8] Wang XZ, Zhang XY, Wang Y. The approach to stability of the three-stage servo valve. *Chin.Hydraul.Pneumat.* 7 ( 2001) 9-11.
- [9] Xu YM. Analysis of null high-frequency free-running oscillation of 3-stage electro-hydraulic servo valve. *J.Wuhan Univ.Sci.Technol. (Nat.Sci.Ed.).* 1 ( 2008) 50-53.
- [10] Song XB. Dynamic performance simulation of three-stage electro-hydraulic servo valve. Academic Symposium on Pressure Processing Equipment, Beijing, 2014, pp. 13–15.
- [11] Liu XC, Huang QT, Cong DC. Analysis of performance effect factors of three-stage electro-hydraulic servo valve. *J.Computers.* 4 (2009) 1216-1222.
- [12] Somashekhar SH, Singaperumal M, Kumar RK. Mathematical modelling and simulation of a jet pipe electro hydraulic flow control servo valve. *Proc.Inst.Mech.Engineers, Part I (J.Sys. Control Eng.).* 221 ( 2007) 365-382.
- [13] Li SG, Hu LM, Cao KQ, et al. Modeling and simulation of dynamic characteristics of the force feedback jet-pipe servo valve. *Fire Control & Command Control.* 42 (2017) 91-96.
- [14] Xu YM. Analysis and design of electro-hydraulic proportional control system, Mechanical Industry Press, Beijing, 2005, pp. 8–18.
- [15] Liu BY. Dynamic simulation of electromechanical system: based on MATLAB/Simulink , China Machine Press, Beijing, 2011, pp. 1–18.
- [16] Zhang Y. Research on the modeling and simulation of jet pipe servo valve, Northwestern Polytechnical University, Xi'an, 2015.
- [17] Zhao KY, Yuan ZH, Zhang Y. Analysis of jet pipe servo valve feedback spring components. *China Mech.Eng.* 19 ( 2013) 2606-2610.
- [18] Wang Y. Mathematical model construction and analysis of jet pipe servo valve, Lanzhou University of Technology, 2012.
- [19] Yin YB, Fei CH, Hu YT. Characteristics of torque motor of jet-pipe servovalve under vibration environment. *Fluid Power Transmiss.Control.* 6 ( 2014) 1-4.
- [20] Yin YB, Pham XHS, and Zhang X. Dynamic stiffness analysis for the feedback spring pole in a jet pipe electro-hydraulic servo-valve. *J.Univ.Sci.Technol.China.* 9 ( 2012) 699-704.